Fe-doped $CuInSe_2$: An *ab initio* study of magnetic defects in a photovoltaic material

Jean-Marc Raulot and Christophe Domain
Electricité de France–Recherche and Développement, Département MMC, Les Renardières, F-77818 Morêt sur Loing Cedex, France

Jean-François Guillemoles*
Institute for Research and Development of Photovoltaic Energy (IRDEP), Unité mixte de Recherche de Electricité de France, du Centre National de la Recherche Scientifique et de l'Ecole Nationale Supérieure de Chimie de Paris, 6 quai Watier, F-78401 Chatou, France

(Received 30 March 2004; revised manuscript received 27 July 2004; published 7 January 2005)

Iron substitution in $CuInSe_2$ could have important implications either for photovoltaic or spintronic applications. To better understand the Fe effects, we have performed density functional calculations on the $CuInSe_2$ chalcopyrite as well as on Fe-doped derivative compounds with different concentrations and geometries. The defect formation energies of Fe_{In} and Fe_{Cu} substitutions for different Fe/metal concentrations (6.25% to 100%) have been determined and we have shown that these energies fluctuate with the Fe content depending on concentration and magnetic ordering. In these Fe-substituted adamantine structures, the antiferromagnetic state has been found to be most of the time more stable than the ferromagnetic state. The magnetic moment of the iron atom was found to slightly decrease with the amount of substituted Fe. The antiferromagnetic to ferromagnetic transition temperatures have been determined by Monte Carlo methods and have been found to be around 100 K in most instances. The analysis of the densities of states was used to make predictions on the influence on photovoltaic performance improvement and on spintronic properties induced by substitutional Fe atoms. For the case of $CuInSe_2$, Fe impurities are expected to impart to the material spintronic properties, depending on the site in which it is substituted, but to degrade its photovoltaic properties.

DOI: 10.1103/PhysRevB.71.035203 PACS number(s): 75.50.Pp, 71.20.−b, 71.55.Ht, 75.10.Hk

I. INTRODUCTION

The ternary I-III-VI_2 compound $CuInSe_2$ (CIS) is a member of the chalcopyrite semiconductor family. Its structural, electrical, and optical properties make it a promising material for photovoltaic applications.[1–3] Indeed CIS and related compounds $Cu(In,Ga)(S,Se)_2$, using thin film technology, are one of the most promising solutions for the production of economically competitive photovoltaic energy with conversion efficiencies up to 22.5%.[4–8]

However, this solution could run short as indium is not a common element in the earth's crust, with only 300 t/yr extracted. For photovoltaic (PV) application, this means that the maximum production of solar modules based on that technology would be limited to about 7 GW_c/yr (Ref. 9) with reasonable assumptions for device structures and performances, and assuming that all In production is consumed for CIS photovoltaic device manufacturing. It is therefore of strategic importance to investigate whether In can be substituted by another more abundant element such as Fe while retaining the properties that make CIS attractive for PV applications.[10] Note that Fe is also an impurity found in CIS films and crystals.[11] Many compounds with a similar structure have also been proposed for spintronic applications.[12–14] This makes it also interesting to study the behavior of magnetic impurities in this system.

In the context of a single material finding applications in several domains, it is thus interesting to investigate whether magnetic and photovoltaic properties have an influence on one another, and specifically, if the presence of iron, or any magnetic impurity, are detrimental for PV properties or on the contrary can be beneficial, something which to the best knowledge of the authors has not yet been investigated.

A priori, a good spintronic material is expected to have poor PV properties because spintronic material requires a metallic semiband (in one spin direction) with a semiconductor semiband (in the other direction), whereas good PV performances requires not only a fully semiconducting character but also a low nonradiative electron-hole recombination rate: the lifetime of the excited photocarriers is one of the major issues for the selections of a PV material. Therefore, magnetic impurities are expected to induce poor PV properties in the material because of the occurrence of the metallic semiband at large concentration and also because of the possible recombination through midgap levels at low concentration.

These subgap states would act, as in nonmagnetic semiconductors, both in enhancing subgap absorption of photons (beneficial effect) and recombination (deleterious effect). The two effects are not independent of course because of the microreversibility principle,[15–18] which states that the probability of the forward reaction is the same as that of the backward reaction. Only in very special cases are (very idealized) midgap impurities expected to yield some improvement of the material's performances to the lifetime of trapped carriers and on the optical cross sections of the occupied or empty defect. One has to get close to the radiative transition limit (i.e., when all the transitions are done through the creation or the annihilation of a photon) to expect an improvement.

Progress in the direction of the recombination reduction can be achieved by enhancing the electron-hole separation, like in a heterojunction [Fig. 1(a)]. Another way of reducing the recombination rate is by blocking the transition, at first order, for instance, because it involves spin flip, as illustrated in Fig. 1(a). The abscissa is no longer the spatial coordinate (as in the heterojunction case) but the spin state. This pro-

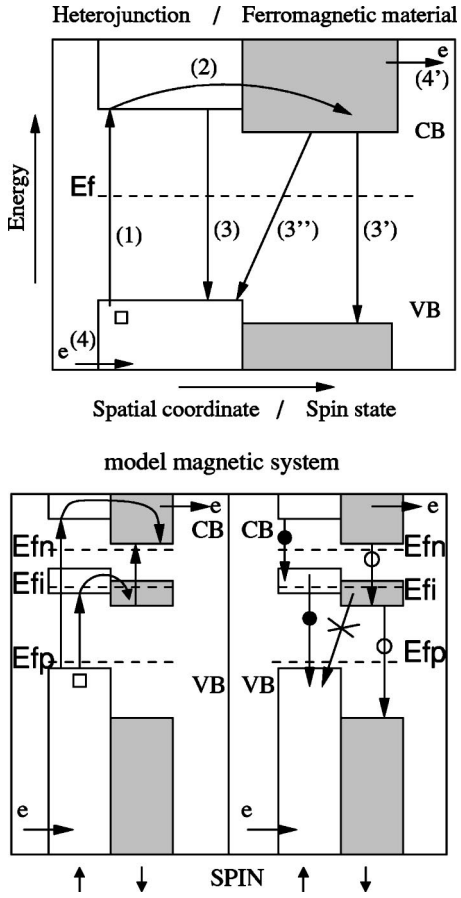

FIG. 1. (a) Schematic electronic transition for an heterojunction, which can be seen as a ferromagnetic material. (1) e^--h^+ pair generation, e.g., via phonon absorption, (2) e^- transport, (3) (3') e^--h^+ recombination, (3") e^--h^+ recombination inhibited, (4') current injection. (b) Schematic electronic transition of a model magnetic system. The symbols on the arrows are as follows: crosses correspond to small recombination matrix elements, open (filled) circles for low initial state electron (final state hole) occupation probability. The horizontal arrows represent the current flow in an operating device.

cess, to be effective, implies that process (2) in Fig. 1 is much faster than (3). The utilization of such ferromagnetic systems pushes to the limit the concept of interpenetrated heterojunction, used for instance in polymer electronics and polymer photovoltaics.[19,20] This possibility can also be extended in both cases (heterojunction and ferromagnetic materials) to multiband systems [Fig. 1(b)]. The cross in Fig. 1(b) indicates the hole-electron recombination with the electron spin inversion (spin-up case) or hole spin inversion (other cases). Arrows with circle indicate recombination rates impeded because few electrons (filled circle) or holes (open circle) with the correct spin are available for the transition to occur. The fastest recombination paths are, in principle, those not involving spin inversion. Therefore the recombination path with crosses could be of negligible influence in most favorable cases.

Of course, adding magnetic elements in a solid will bring many changes that will bear on the efficiency of photovoltaic conversion such as band gap modification or strength of optical absorption, which are not specific to the magnetic character of the element introduced. These well known effects can play both ways and increase or decrease the PV performance.

Let us now turn then to the specific influence of the spin states and magnetic order on photovoltaic energy conversion whose influence has so far never been investigated to the best of our knowledge. The positive effect of the introduction of a magnetic element has been experimentally observed by Chou *et al.*[21] in ZnSe. They display an unexpected long hole spin relaxation time associated with the strain splitting of the valence band. This indicates that carrier lifetimes can be extended in such systems.[22]

If lifetimes could be extended long enough so that optical pumping could proceed, as proposed for instance in Ref. 23 for multiband systems and shown in Fig. 1, then the material efficiency could reach values as high as 62% provided the energy level separation is well matched to the solar spectrum. Although multiband and multilevel systems[18,23,24] have been proposed previously, experimental systems enabling collection of the gains are still lacking because the losses in such systems are very likely to overcome the gains. We propose that magnetic doping could be used to implement this efficiency enhancement. The occurrence of this recombination bottleneck depends on the ratio of the scattering time with magnetic impurities yielding the spin polarization versus the photogenerated carrier lifetime, on the efficiency of the polarization of the carriers via scattering by magnetic impurities, and on the band structure. Stabilization of the exited states in the intermediate levels (through spin flipping) can be achieved using the splitting of the density of states (DOS) in spin-up and -down states as shown in Fig. 1. This would hinder spontaneous recombination so that efficient net absorption from the intermediate state could in principle be enhanced. There is an analog to this effect in organic fluorescent dyes where the triplet state, energetically more stable than the singlet state, imparts to the system long decay times (i.e., an extended excited lifetime) to ground state because the relaxation process involves spin flipping and therefore some spin-orbit interactions.

In the present work, we have chosen an *ab initio* approach to study the modification of the DOS induced by Fe in CIS so as to evaluate the potential of these compounds either for PV or spintronic applications. We have also investigated the stabilities of the various possible compounds formed and their magnetic order.

The $CuInSe_2$ compound has been studied experimentally and theoretically by several groups.[1–6] Nowadays, these studies have focused on the impact of structural modifications on its optical and electronic properties. Indeed, a large variety of isolated point defects can be formed, which generally decrease the efficiency. In particular, Zunger and co-workers[25–27] have investigated the isolated intrinsic point defects (V_{Cu}, V_{In}, Cu_{In}, Cu_i, where V stands for a vacancy, i for an interstitial, and the subscript stands for the crystallographic site of the related defect or substituted atom) and mixed point defects ($2V_{Cu}+In_{Cu},\ldots$) in $CuInSe_2$. They observed that some of these defects have very low formation energies. The vacancy formation energy $[E_{for}(V_{Cu})]$ equals 0.6 eV and the mixed di-copper-vacancy In_{Cu} complex for-

mation energy $[E_{for}(2V_{Cu}+In_{Cu})]$ equals 0.33 eV.[25] Other *ab initio* calculations confirmed these trends. For instance, using pseudopotentials and 32-atom supercells within the local density approximation (LDA), we obtained $E_{for}(V_{Cu})=0.47$ eV and $E_{for}(2V_{Cu}+In_{Cu})=0.17$ eV.[28,29] Some surface properties have also been addressed: surface states and the (112) surface electronic structure,[30] or the (110) surface transformation from nonpolar surface to polar facet surface.[31] However, few theoretical efforts have been related to extrinsic elements in chalcopyrites.

First-principles calculations have shown that the preferential site of Mn in Cu based $CuMX_2$ chalcopyrite depends strongly on the Cu and *M* cation chemical potentials.[32] It has also been shown that Mn substitutes for Cu in the *M*-rich region, and for *M* with in the Cu-rich or *M*-poor regions of the phase diagram. Furthermore Mn reduces the stability domain of the chalcopyrite in the phase diagram. Picozzi *et al.*[33] have performed *ab initio* calculations in the Mn-doped $CuGaS_2$ chalcopyrite structures and showed the important role of Mn_{Ga} substitutions on the magnetic properties of this material. Their calculations showed that the ground state of these compounds is ferromagnetic rather than antiferromagnetic. For spintronics applications, a large amount of experimental and theoretical work was carried out on binary semiconductors such as GaAs.[33,34] The substitution of Ga by Mn, which is a transition metal, leads to a ferromagnetic ground state and, for low Mn concentration, a semimetallic character is even observed. If Fe rather than Mn is substituted, no ferromagnetic ground state is generally found.[35]

We assume that the ionic charge of the atoms is 1+ for copper atom, 3+ for the indium atom, and 2− for the selenium atom. This charge distribution is in agreement with the accurate calculation of the Born charges realized by Parlak and Eryigit:[36] 0.86 for Cu, 2.46 for In, and −1.66 for Se. Thus, the defect physics of Fe_{In} and Fe_{Cu} may have different behaviors as they have different second-neighbor shells.

In this paper, we have studied the Fe-doping effects on the $CuInSe_2$ compound. Cationic substitutions by Fe have been considered from low concentration (6.25% of Cu or In atoms substituted, equivalent to 1 wt % Fe concentration) up to $FeInSe_2$ and $CuFeSe_2$ compounds and we have analyzed the effect of the substitution on the energetic properties (substitutional energy) and the magnetic properties of the compounds. From this analysis, the opportunity of Fe doping in $CuInSe_2$ is discussed. Ferromagnetic (FM) and antiferromagnetic (AFM) states for Fe-substituted compounds have been investigated and the associated transition temperatures have been deduced. Finally, the influence of the magnetic state on the optoelectronical properties of the chalcopyrite compounds is discussed.

II. METHODS

A. Computational method

We performed *ab initio* calculations based on the density-functional theory[37] (DFT) and using the Vienna *ab initio* software package[38–41] (VASP). The ultrasoft pseudopotentials of Vanderbilt type[42] of the VASP library and a plane wave basis set were utilized. The pseudopotentials used were generated within the gradient conjugated approximation (GGA) [Perdew and Wang[43] (PW91)] to describe the exchange-correlation energy. In the pseudopotential approach, core electrons that do not participate in the bonding character of the material are frozen and only valence electrons are taken into account. For the pseudopotentials used, the electronic configurations were, respectively, $[Ar]4s^13d^{10}$, $[Kr]5s^25p^1$, $[Ar]4s^24p^4$, and $[Ar]4s^13d^7$ for copper, indium, selenium, and iron. In this work, the kinetic energy cutoff chosen was 240 eV and a Monkhorst-Pack[44] grid was used to sample the Brillouin zone. The dimension of the *k* point grid varies with the cell size in order to keep a constant *k* point density in the Brillouin zone. The supercell approach with periodic boundary conditions was used. In the primitive cell that contains two $CuInSe_2$ motifs, convergence is achieved with a grid containing $6\times6\times6$ *k* points. Among the different convergence tests performed to assess the energy cutoff and *k* point mesh used, some comparisons for 240 and 350 eV as energy cutoff and for $6\times6\times6$ and $12\times12\times12$ *k* point mesh are presented in Table I. Therefore, for a 64-atom supercell $(Cu_{16}In_{16}Se_{32})$, we have used a $3\times3\times3$ *k* point grid. The calculation is semirelativistic and for the Fe-doped $CuInSe_2$ the spin polarization is taken into account. Both ferromagnetic and antiferromagnetic states have been considered for Fe atoms. All structures have been relaxed using the conjugate gradient algorithm. Both the atomic position and supercell volume have been optimized, except for the largest supercells (64 atoms) for which only the atomic positions have been relaxed. After relaxation, the forces on the atoms were checked to be lower than 0.02 eV/Å. From these calculations, energies, magnetic moments, and relaxed structures have been analyzed. In addition, the total density of states as well as the partial density of states (PDOS) has been determined. To calculate the PDOS, the projection of the electronic density onto the atomic orbital requires definition of the radius of the sphere on which to project. The following atomic Wigner-Seitz radii 1.312, 1.677, 1.312, and 1.302 Å, respectively, for Cu, In, Se, and Fe atoms were chosen.

TABLE I. Convergence test on the energy cutoff and *k* point mesh. Results on the equilibrium volume (Ω) of $CuInSe_2$ per motif, and energy differences between the AFM and FM states ($E_{\uparrow\downarrow}-E_{\uparrow\uparrow}$) of $FeInSe_2$ and $CuFeSe_2$ per motif are given for 240 and 350 eV energy cutoff, and $6\times6\times6$ and $12\times12\times12$ *k* point mesh.

Cutoff (eV)	*k* point	$\Omega(CuInSe_2)$ (Å^3)	$\Delta E(FeInSe_2)$ (eV)	$\Delta E(CuFeSe_2)$ (eV)
240	$6\times6\times6$	101.0	−0.119	−0.345
240	$12\times12\times12$	100.9	−0.120	−0.341
350	$6\times6\times6$	101.2	−0.123	−0.343

B. Defect calculation method

The defect calculations are performed by replacing one or several Cu or In atoms by Fe atoms in different size supercells containing 8, 16, 32, or 64 atoms. The 8-atom cell with the following lattice vectors, $\{(-a/2,a/2,c/2),(a/2,-a/2,c/2),(a/2,a/2,-c/2)\}$, has a $I\bar{4}2d$-D_{2d}^{12} (122) space

TABLE II. Chalcopyrite $CuInSe_2$($I\bar{4}2d$-D_{2d}^{12}-122) structural parameters. Ω is the volume by motif.

	Experiment		Theory		
	Reference 45	Reference 46	This work	FLAPW[a]	Pseudopotential[b]
a(Å)	5.781	5.782	5.859	5.768	5.562
c(Å)	11.642	11.619	11.765	11.628	11.134
u	0.226	0.235	0.220	—	0.237
Ω(Å^3)	97.3	97.1	101.0	96.6	86.1

[a]Full potential linearized augmented plane wave; Ref. 25.
[b]Referene 36.

group. For the cell containing 16 atoms $\{(a,0,0), (0,a,0), (0,0,c)\}$ there are two cases: if the cell has a reverse center of symmetry the space group is $I\bar{4}$-S_4^2 (82); otherwise the space group is $P4$-S_2^1 (81). For these cells, we optimized the structure (lattice parameters and atomic positions) to obtain the equilibrium geometry (corresponding to the total energy minimum). The cell containing 32 atoms has lattice vectors $\{(a\sqrt{2},a\sqrt{2},0), (a\sqrt{2}, -a\sqrt{2},0), (0,0,c)\}$, and both the atomic positions and the supercell volume have been optimized. For 64 atoms, only the atomic positions have been relaxed at fixed volume with the lattice vectors $\{(2a,0,0), (0,2a,0), (0,0,c)\}$. The a and c lattice parameters are the equilibrium parameters obtained after full relaxation of the 16-atom supercell without any defect.

The formation energy of a defect α is calculated as follows:[25,26]

$$\Delta H_f = \delta E(\alpha) + n_{\mathrm{Cu}}\mu_{\mathrm{Cu}} + n_{\mathrm{In}}\mu_{\mathrm{In}} + n_{\mathrm{Fe}}\mu_{\mathrm{Fe}}, \tag{2.1}$$

where

$$\delta E(\alpha) = E(\alpha) - E(\mathrm{CuInSe_2}) + n_{\mathrm{Cu}}\mu_{\mathrm{Cu}}^{solid} + n_{\mathrm{In}}\mu_{\mathrm{In}}^{solid} + n_{\mathrm{Fe}}\mu_{\mathrm{Fe}}^{solid}. \tag{2.2}$$

$E(\alpha)$ and $E(\mathrm{CuInSe_2})$ are the total energies of the unit cell with and without the defect, respectively. $\mu_{\mathrm{In}}^{solid}$ and $\mu_{\mathrm{Fe}}^{solid}$ are the total energy of ground state solid In (tetragonal) and solid Fe (centered cubic). The n_i are the number of atoms transferred from the supercell to the reservoir in order to create the defect. μ_{In} and μ_{Fe} represent the chemical potential of the indium atom and the iron atom, which corresponds to the energy variation of an atom to or from a chemical reservoir, which is not necessary in the solid ground state. To maintain the accuracy by error cancellation, $E(\alpha)$ and $E(\mathrm{CIS})$ are computed with the same grid of k points and the same kinetic energy cutoff for the same supercell size.

Fe-doped $CuInSe_2$ can also be considered as a defined compound along the pseudobinary lines $CuInSe_2$-$FeInSe_2$ or $CuInSe_2$-$CuFeSe_2$. The mixing energy for the Fe substituted on Cu sites is given by

$$\Delta E(\mathrm{Cu_{1-x}Fe_xInSe_2}) = E(\mathrm{Cu_{1-x}Fe_xInSe_2}) - (1-x)E(\mathrm{CuInSe_2}) - xE(\mathrm{FeInSe_2}), \tag{2.3}$$

and for Fe on In sites:

$$\Delta E(\mathrm{CuIn_{1-x}Fe_xSe_2}) = E(\mathrm{CuIn_{1-x}Fe_xSe_2}) - (1-x)E(\mathrm{CuInSe_2}) - xE(\mathrm{CuFeSe_2}). \tag{2.4}$$

Note that this relation is independent of the chemical potential of the elements.

III. RESULTS

A. Optimized structures

The chalcopyrite structure is derived from the cubic zinc-blende structure, which contains, however, only one type of cation (space group T_d^2). The presence in the chalcopyrite structure of two different cations (Cu and In) ordered in the half tetrahedral sites yields a doubling of the zinc-blende unit cell along the the c direction. The anion (Se) has four first neighbors: two copper and two indium atoms. Table II gives the calculated and the experimental lattice parameters. The structure is optimized by alternatively repeating the relaxation of the ions in order to minimize the forces, the variation of the volume, and the shape of the supercell to minimize the stress tensor. The a and c parameters are overestimated by approximately 1.2%. This yields a volume error of 3%, which is within the error usually obtained with DFT methods. The distance between the copper and selenium atoms is smaller (2.41 Å) than the distance between the indium and selenium atoms (2.63 Å). The structure exhibits channels along the $\langle 110\rangle$ and $\langle 102\rangle$ directions. Our calculations in Table II correctly describe the chalcopyrite structure.

The structural parameters of $CuFeSe_2$ and $FeInSe_2$ in the AFM and FM states are reported in Table III. $CuFeSe_2$ is a tetragonal mineral called eskebornite, in the chalcopyrite group. However, to our knowledge, the $FeInSe_2$ compound has not been characterized experimentally.

For the small supercell calculations (8 and 16 atoms), an increase of the Fe_{In} substitution concentration leads to a strong decrease of the cell volume (the $CuFeSe_2$ volume cell is 15% smaller than the $CuInSe_2$ cell). The distance between an indium atom and its selenium neighbor atoms is about 2.63 Å, while the distance between an iron atom and its four selenium neighbor atoms is 2.42 Å, which is very similar to the Cu-Se distance (2.41 Å). Consequently, the tetrahedron defined by Fe atoms and four Se atoms is close to a perfect one for $CuFeSe_2$ and this chalcopyrite compound has a c/a ratio almost equal to 2. Moreover, a large variation of the

TABLE III. Antiferromagnetic and ferromagnetic structures of $CuFeSe_2$ and $FeInSe_2$($I\bar{4}2d$-D_{2d}^{12}-122) structural parameters. Ω is the volume by motif.

Compound	$CuFeSe_2$ AFM	$CuFeSe_2$ FM	$FeInSe_2$ AFM	$FeInSe_2$ FM
a(Å)	5.550	5.557	5.971	5.947
c(Å)	11.139	11.154	11.984	11.937
u	0.256	0.233	0.193	0.204
Ω(Å^3)	85.8	86.1	106.8	105.6
d(Fe-Se)(Å)	2.39	2.41	2.41	2.43

angles is observed (Fig. 2), in particular, the Se-Fe-Se angles with the variation of the Fe_{In} percentage converge to 109.5° for $CuFeSe_2$, whereas for the Fe_{Cu} substitution, the angle variations are smaller ($\simeq 1°$) than those for Fe_{In}($\simeq 5°$).

The evolution of the *a* and *c* lattice parameters as a function of the Fe content are reported in Fig. 3 for Cu as well as In substitution. As Fe's size is intermediate between that of Cu and In, the lattice parameters decrease in the case of Fe_{Cu} and increase for Fe_{In}. To our knowledge, the only experimental lattice parameter measurements available have been performed by Sanchez Porras *et al.*[47] with up to 500 wt ppm Fe (i.e., 0.3%). However, no clear variation of the lattice parameters could be established, possibly because the variation is too small compared to the accuracy of the experimental methods. Nevertheless, our calculations indicate a clear and linear variation of the lattice parameters with Fe content, consistent with the relative Fe/Cu and Fe/In atomic size ratios. For a given amount of Fe, the ferromagnetic and antiferromagnetic states structures are almost identical and the relative relaxation is negligible compared to the variation of the lattice parameters or angles with the Fe content.

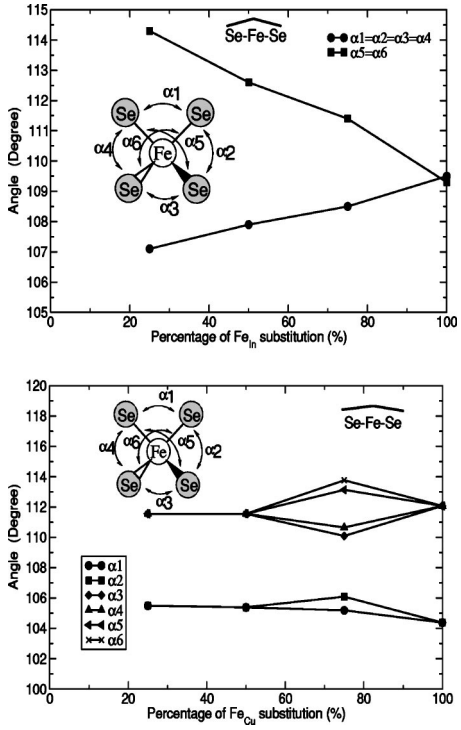

FIG. 2. Variation of the ∠Se-Fe-Se angles with (a) Fe_{In} and (b) Fe_{Cu} concentration (FM state). For pure $CuInSe_2$, the Se-In-Se angles are 108° and 112.5°, the Se-Cu-Se angles are 106° and 111.2°.

B. Defect energies

The formation energies of the compounds obtained by substituting Cu or In atoms by Fe atoms in $CuInSe_2$ have been calculated. The results are presented in terms of mixing enthalpies of $Cu_{1-x}Fe_xInSe_2$ compounds made from $CuInSe_2$ and $FeInSe_2$, and of $CuIn_{1-x}Fe_xSe_2$ compounds made from $CuInSe_2$ and $CuFeSe_2$ along the pseudobinary line (Fig. 4). Results for the AFM and for the FM configurations are represented, taking as a reference the most stable magnetic state, i.e., the AFM configuration for the Fe compounds. The Fe repartition and the AFM state configuration with the notation of the different configuration is given in Fig. 5 using relations (2.3) and (2.4). The antiferromagnetic configurations are found to be more stable than the ferromagnetic ones for the $CuIn_{1-x}Fe_xSe_2$ compounds with Fe concentration larger

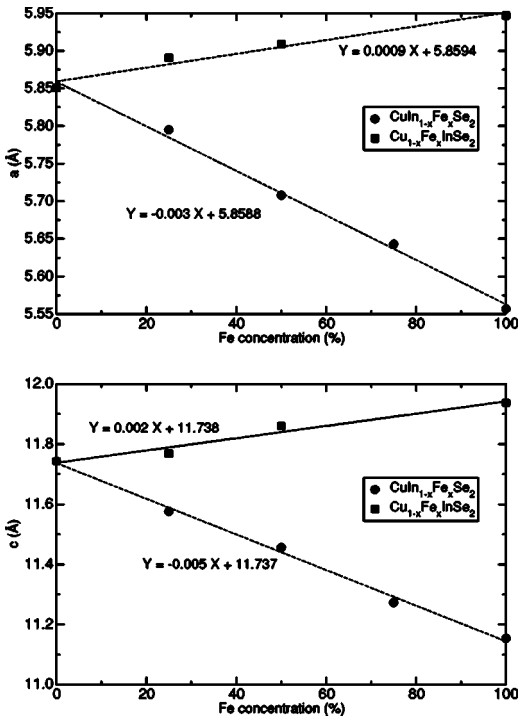

FIG. 3. Evolution of the *a* and *c* lattice parameters as a function of Fe substitution content on Cu and In sites (FM state).

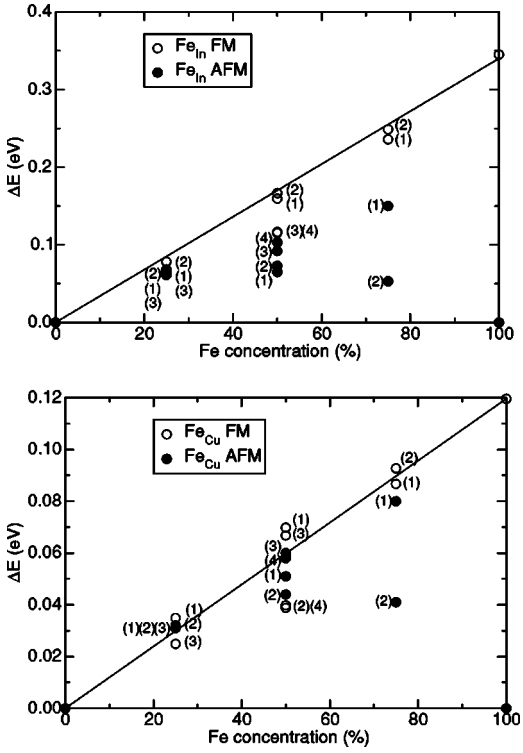

FIG. 4. Variation of mixing energy (eV) with Fe magnetic center concentrations. (a) Fe_{In} substitution: $\Delta E = E_{CuIn_{1-x}Fe_xSe_2} - xE_{CuInSe_2} - (1-x)E_{CuFeSe_2}$. (b) Fe_{Cu} substitution: $\Delta E = E_{Cu_{1-x}Fe_xInSe_2} - xE_{CuInSe_2} - (1-x)E_{FeInSe_2}$. For both $CuFeSe_2$ and $FeInSe_2$ the reference energy (0) is the AFM state.

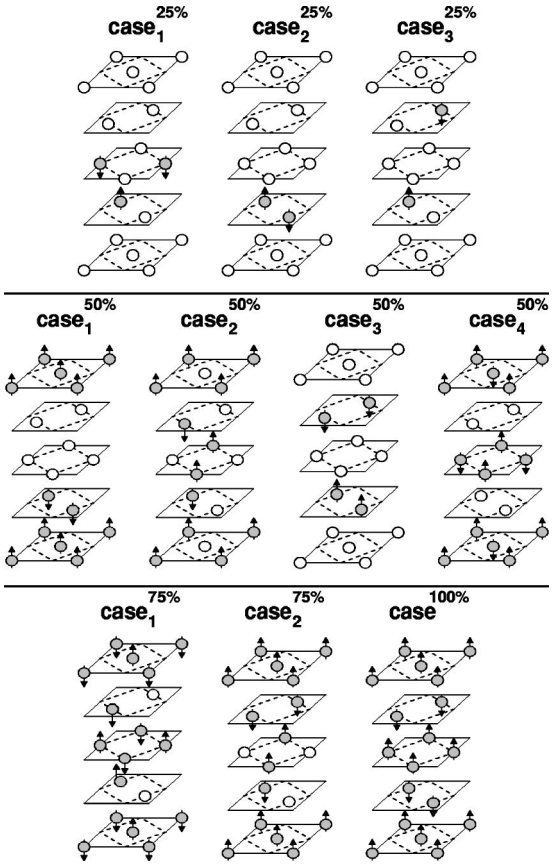

FIG. 5. Antiferromagnetic configurations (32-atom supercell represented and we only present one cation type). The figures of the In and Cu cation substitutions are similar with $\left(\frac{1}{2},\frac{1}{2},\frac{1}{2}\right)$ translation.

than 25% (the energy difference being rather small for Fe concentration below 25%). For the $Cu_{1-x}Fe_xInSe_2$ compounds, the energy differences between the antiferromagnetic and ferromagnetic cases are not significant.

In the case of Fe_{In} substitutions two behaviors are observed depending on the magnetic state. In the FM states, the mixing energy is negative and compounds with different Fe concentration on In sites may be expected, whereas, for the AFM state, a tendency to demixion into end-line compounds is found. This is the stable state, in absence of an applied magnetic field. For 50% of substitution, the most stable cases are, respectively, the $case_1^{50\%}$, $case_2^{50\%}$, $case_3^{50\%}$, and $case_4^{50\%}$ configurations (Fig. 5). Only for some special configurations ($case_4^{50\%}$) may an FM state be stable ($case_4^{50\%}$ and all the cases with 25% Fe content). The most stable case ($case_1^{50\%}$) is composed of two nearest-neighbor (001) planes, one plane containing the spin-up Fe atoms and the other plane with the spin-down Fe atoms. The most unstable cases are the cases where the two planes are not nearest neighbors and where there are both spin-up and -down Fe atoms in the same (001) plane. Indeed, two antiferromagnetic iron atoms in nearest-neighbor positions reduce the total energy.

For Fe_{Cu} a 50% Fe compound could be stable but the AFM and FM states have very close energies and the present calculation could not determine the most stable of the two. Consequently a mix of both AFM and FM states may be expected and along the pseudobinary line $CuInSe_2$-$FeInSe_2$ a solid solution can be expected on the Cu cation lattice (Fig. 4). Because all concentration have total energies close to the $CuInSe_2$-$FeInSe_2$ tie line, a strong site disorder can be expected in these compounds.

C. Magnetic properties

We have examined the variation of the local magnetic moment μ_B per iron atom as a function of the Fe_{In} substitution concentration. The local magnetic moment per iron atom is calculated by subtracting from the spin-up electronic density the spin-down electronic density within a sphere centered on the atomic site, and of radius the atomic Wigner-Seitz (WS) radius r ($r_{WS}^{Fe}=1.302$ Å). The magnetic moment lies between 3.4 and 3.5 μ_B for Fe_{In} substitution. For the Fe_{Cu} substitution, the magnetic moment per iron atom varies from 2.98 to 3.08 μ_B. All the magnetic moments are not strictly located on the Fe atoms. Indeed, the first-nearest-neighbor Se atoms have a local magnetic moment of $\simeq 0.1\mu_B$ (with $r_{WS}^{Se}=1.312$ Å) per Se atom, which may come from the Fe-Se covalent bonding. The other atoms carry much smaller magnetic moments, which are in fact insignificant.

The standard Heisenberg model[48] was used to describe the exchange magnetic interactions between spins on Fe atoms. The effective Heisenberg Hamiltonian is:

TABLE IV. Energy difference (ΔE) per Fe atom (in eV) between the antiferromagnetic and ferromagnetic configurations, and transition Néel T_N or Curie temperature T_C (in K) for the different configuration studied. The uncertainty of these Metropolis Monte Carlo results is ±5 K.

Case	$\Delta E(Fe_{Cu})=E_{\uparrow\downarrow}-E_{\uparrow\uparrow}$	$T_C(Fe_{Cu})$	$\Delta E(Fe_{In})=E_{\uparrow\downarrow}-E_{\uparrow\uparrow}$	$T_C(Fe_{In})$
$case_1^{25\%}$	−0.02	-	−0.05	-
$case_2^{25\%}$	−0.01	40 (N)	−0.01	30 (N)
$case_3^{25\%}$	0.02	70 (C)	−0.03	60 (N)
$case_1^{50\%}$	0.04	150 (C)	−0.11	120 (N)
$case_2^{50\%}$	−0.04	50 (N)	−0.18	400 (N)
$case_3^{50\%}$	0.04	40 (C)	−0.04	50 (N)
$case_4^{50\%}$	0.02	100 (C)	−0.02	50 (N)
$case_1^{75\%}$	−0.01	<50	−0.12	55 (N)
$case_2^{75\%}$	−0.07	35 (N)	−0.26	100 (N)
$case^{100\%}$	−0.12	600 (N)	−0.34	1000–1200 (N)

$$H_{eff} = -\sum_{i\neq j} J_{ij}\vec{e}_i \cdot \vec{e}_j, \tag{3.1}$$

where J_{ij} is the exchange interaction between two Fe sites (i,j) and $\vec{e}_i$ is the unit vector pointing in the direction of the magnetic moments at the site i. From the energy difference between the FM and AFM ground states, the coupling parameter J and the associated transition temperature have been determined. In almost all the cases investigated here, the AFM ground state is more stable than the FM ground state. The different substitutional configurations of the Fe atoms having complicated geometries, the Néel and Curie transition temperatures have been obtained directly by standard Metropolis Monte Carlo simulation.

The energy E of a configuration is given by

$$E = \sum_n \alpha_n J_n(x), \tag{3.2}$$

where J_n is the exchange interaction energy between the nth-nearest Fe neighbors and α_n is the associated number of pairs. Table IV gives the energy variation $\Delta E_{\uparrow\downarrow}$ between the ferromagnetic state and the antiferromagnetic state of a same configuration and the associated exchange interaction terms. The relation between the energy difference and the J terms is given by

$$\Delta E(\uparrow\downarrow) = E(\uparrow\downarrow) - E(\uparrow\uparrow) = 2\sum_n \alpha_n J_n(x). \tag{3.3}$$

$J_n(x)$ is assumed to decay as a power law $J_n(x)=sx^{-\lambda}$, with $s=1$ for the FM ground state and $s=-1$ for the AFM ground state. The obtained values for the λ exponent are close to 3 (Table V) for almost all the configurations explored.

These $J(x)$ parameters have been introduced in a Metropolis Monte Carlo simulation. A system containing $6\times6\times6$ chalcopyrite unit cells (1728 possible sites) with periodic boundary conditions was simulated. The system size was found not to have a significant effect on the results obtained. The simulation box was first heated up to a high temperature (>1000 K), and then the temperature was made to decrease linearly by 5 K steps until reaching 0 K. All the sites were randomly visited and the spin inversion of a site was accepted according to the Metropolis algorithm. A Monte Carlo step was constituted of one visit of each site, and 500 steps per temperature were made. The Néel transition temperature was determined by the temperature of the transition of the

TABLE V. Expression of ΔE as a function of the coupling term $J_n(x)$ and coupling term parameter s and $\lambda[J(x)=sx^{\lambda}]$ between the antiferromagnetic and ferromagnetic configurations (x in Å).

Case	$\Delta E=2\Sigma\alpha_n J_n(x)$	$s(Fe_{Cu})$	$\lambda(Fe_{Cu})$	$s(Fe_{In})$	$\lambda(Fe_{In})$
$case_1^{25\%}$	$2J(4.1)+4J(7.2)+4J(9.2)+8J(10.9)$	−1	3.554	−1	3.036
$case_2^{25\%}$	$8J(5.8)$	−1	3.632	−1	3.699
$case_3^{25\%}$	$8J(7.2)+16J(10.9)$	1	3.181	−1	3.072
$case_1^{50\%}$	$4J(4.1)+8J(7.2)+8J(9.2)+16J(10.9)$	1	3.510	−1	2.979
$case_2^{50\%}$	$8J(4.1)+8J(7.2)+12J(9.2)$	−1	3.543	−1	2.529
$case_3^{50\%}$	$16J(7.2)+32J(10.9)$	1	3.224	−1	3.192
$case_4^{50\%}$	$16J(5.8)+8J(7.2)+16J(10.9)$	1	3.138	−1	3.108
$case_1^{75\%}$	$8J(4.1)+16J(5.8)+24J(7.2)$	−1	5.183	−1	3.476
$case_2^{75\%}$	$12J(4.1)+24J(7.2)$	−1	3.786	−1	2.931
$case^{100\%}$	$16J(4.1)+32J(9.92)+16J(10.9)$	−1	3.065	−1	2.490

energy of the system from disordered to ordered AFM. The Curie temperature corresponds to the temperature of the transition of the magnetization from FM to AFM. For most of the cases, the final spin order found by Monte Carlo methods was consistent with the order found in our *ab initio* calculations.

The transition temperatures obtained are low as expected from the small energy difference between the FM and AFM states. They are within the range 30–400 K (Table IV) for most of the cases. The transitions are first order except for the configuration case$_1^{25\%}$ for which a second-order transition occurs.

For few configurations, the final AFM order is different from the *ab initio* ordering (case$_1^{50}$ and case$_2^{75}$ for Fe_{In}, case$_1^{75}$ for Fe_{Cu}, and case$_3^{50}$ for both substitutions). The final Monte Carlo order obtained does not converge to a succession of (001) planes (completely substituted) with the same spin. Case$_3^{50}$ decays to case$_4^{50}$ for Fe_{In}. The other configurations converge to another planar spin order. In these cases, our simple pair interaction model does not lead to the ordered structure calculated by *ab initio* and additional terms (such as three-body) may be required. The Néel temperature is higher for the configuration whose AFM-FM energy difference is the largest, and for $CuInSe_2$(case$^{100\%}$) due to the strong AFM coupling, the transition temperature is around 1000 K.

D. Electronic structure

The $CuInSe_2$ partial densities of states provide information on the different interactions between Cu-Se and In-Se. The DOS obtained (Fig. 6 for 0% Fe substitution) is in agreement with the previous calculations of Jaffe and Zunger.[27] The DOS can be decomposed into several parts. At 6 eV below the Fermi level (E_F), the states correspond to a hybridization between In 5*s* states and Se 4*p* states. The states from −5 eV to the Fermi level represent the hybridization of the Cu 3*d* states and Se 4*p* states, In 5*p* states, and Se 4*p* states. The gap of CIS is controlled by the Cu 3*d* and Se 4*p* states (valence band) and the In 5*s* states (conduction band). The DFT method is known to underestimate the band gap value as previously explained.[25]

Figures 6 and 7 show, respectively, the DOS of $CuIn_{1-x}Fe_xSe_2$ and $Cu_{1-x}Fe_xInSe_2$ for 6 values of the Fe concentration. The substitution of Cu by an Fe atom leads to different changes in the electronic structure than the substitution of an In atom.

For the $CuIn_{1-x}Fe_xSe_2$ compounds, new states can be observed in the gap between −3 and −2 eV only in the spin-up band. The number of these states and their width depend on the percentage of Fe substitution. For concentrations larger than 25% the gap is filled. These states represent three electrons (spin up) per Fe atom. For small Fe concentrations (6.25% and 12.5%), some states with the spin-down character just above the Fermi level and up to 0.25 eV can be observed. They represent two electrons per Fe atom [Fig. 8(a)]. (More precisely, at the Fermi level, the spin-up DOS is not strictly 0; for 6.25%, there is less than 0.01 electron with spin up character above the Fermi level, which is not significant.) These changes are no longer present for the high Fe concentration. The spin-up and -down densities of states are overlapped at the Fermi level.

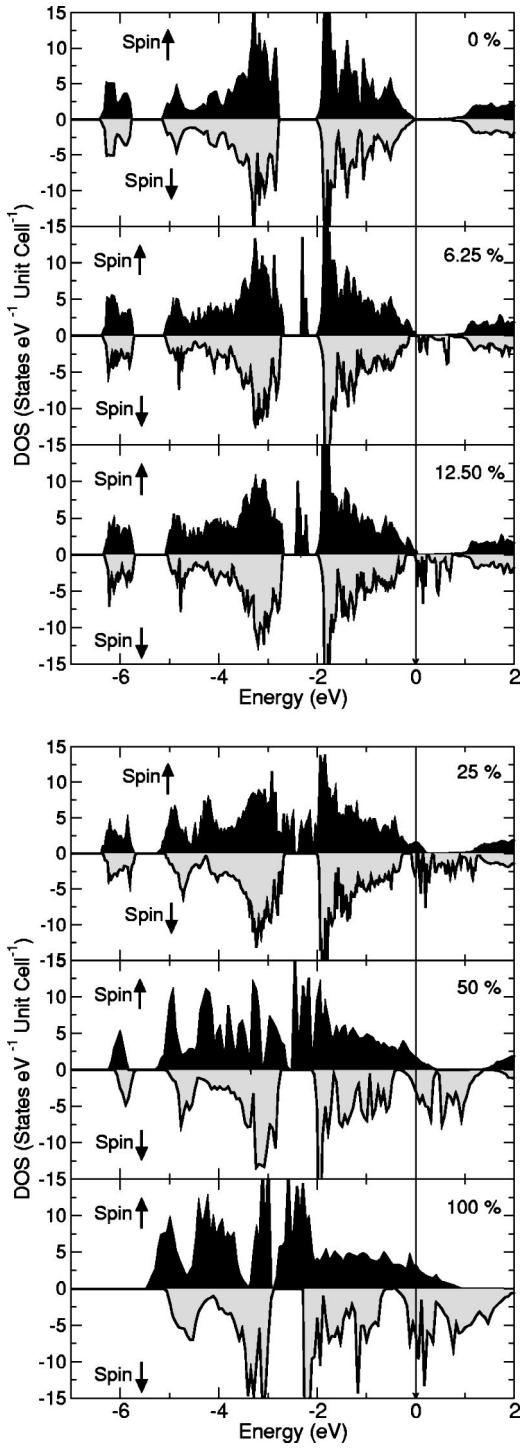

FIG. 6. Density of states of $CuIn_{1-x}Fe_xSe_2$ (FM state).

Fe_{In} defects are intrinsically acceptor defects (see Fig. 6). Increasing the Fe_{In} defect concentration in the $CuInSe_2$ structure creates more and more new levels above the Fermi level (E_F) whereas decreasing the indium atom concentration increases the gap energy by removing the *s* states around 1 eV above E_F. We can observe that the spin-down bands of the iron are totally filled at E_F and the spin-up bands are partially

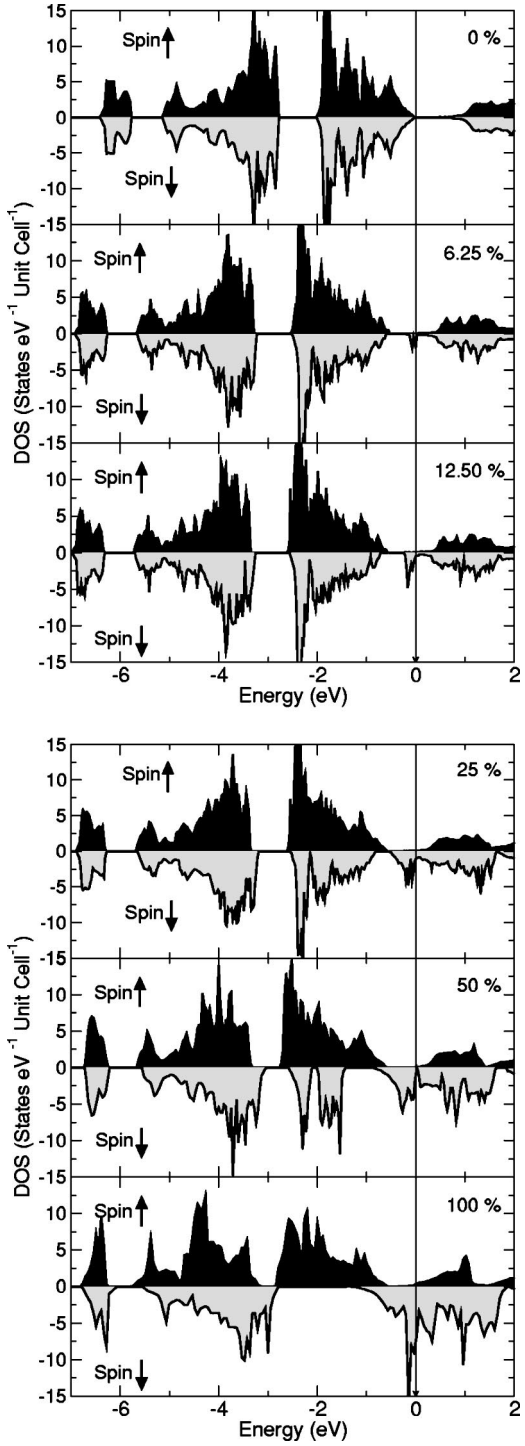

FIG. 7. Density of states of $Cu_{1-x}Fe_xInSe_2$ (FM state).

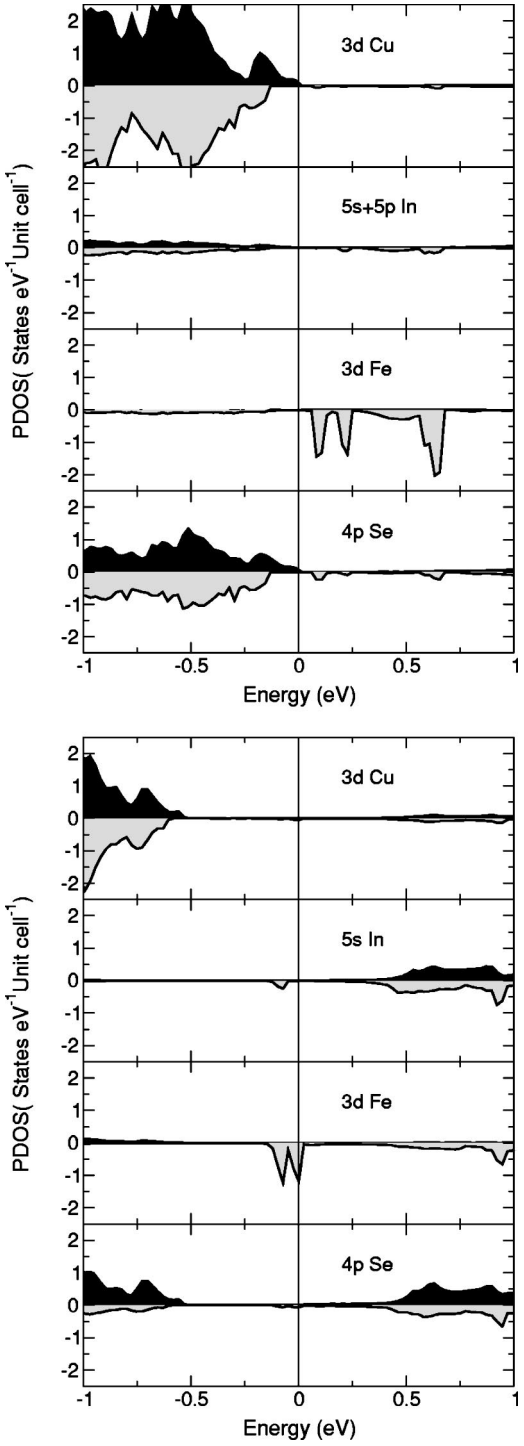

FIG. 8. Partial density of states of (a) $CuIn_{15/16}Fe_{1/16}Se_2$ and (b) $Cu_{15/16}Fe_{1/16}InSe_2$ (FM state).

filled. This effect is responsible for the magnetic moment of the iron atom.

Compared to Fe_{In}, in $Cu_{1-x}Fe_xInSe_2$, no new Fe states are created within the gap in the 3*d* Cu band (from −3 to −2 eV) (Fig. 7). For low Fe concentration (6.25% and 12.5%), the Fe_{Cu} defects are donor defects. At 0.5 eV below the Fermi level, the presence of spin-down states can be observed, however no spin up states are visible. These down states correspond to 2 electrons per Fe atom [Fig. 8(b)]. The typical 3*d* Cu states, usually localized between −5 and −3 eV and between −2 and 0 eV, are shifted by −0.5 eV. Thus, the Fermi level is localized 0.5 eV above the Fermi level of the pure $CuInSe_2$ compound.

In addition, at low Fe concentration, both FM and AFM states have close energies and may coexist and the density of states are represented in Fig. 9 (for 3.1% Fe concentration). For the FM state only electrons with spin-down character are

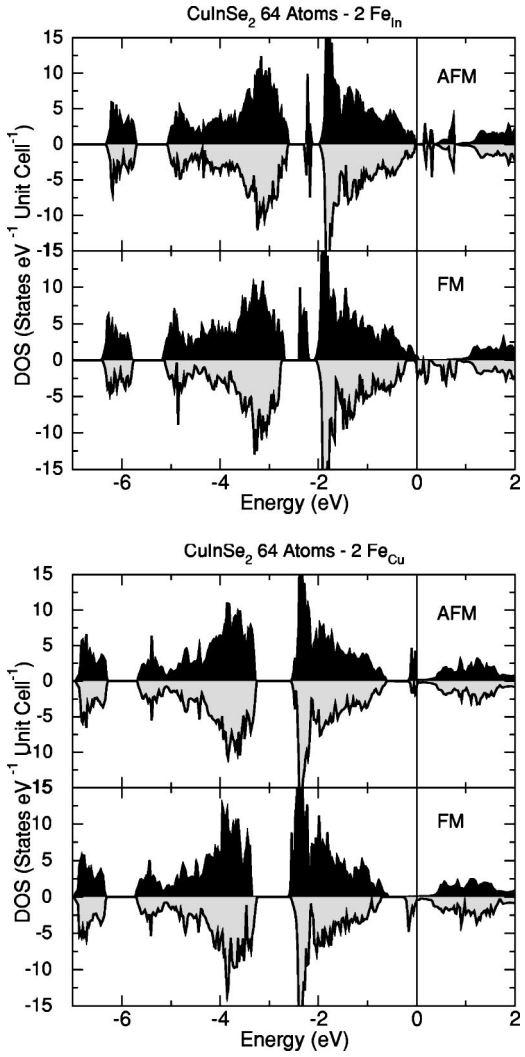

FIG. 9. Density of states of (a) $CuIn_{7/8}Fe_{1/8}Se_2$ and (b) $Cu_{7/8}Fe_{1/8}InSe_2$ (FM and AFM states).

present around the Fermi level, whereas for AFM state, both spin characteristics are present due to the symmetry of the up and down parts of the DOS. Consequently, no spintronic effect can be obtained with the AFM state. Furthermore, the spreading of the two-electron peak is slightly larger for the FM than the AFM states.

IV. DISCUSSION

The formation energies of Cu and In by Fe have also been determined using relations (2.1) and (2.2). These energies correspond to the formation enthalpy at zero chemical potentials ($\mu_{Cu}=\mu_{In}=\mu_{Fe}=0$). For the Fe_{Cu} substitution the formation energies go from 0.80 to 0.86 eV depending on the Fe concentration, and they are lower than that for the Fe_{In} case (formation energy between 1.01 and 1.23 eV). However, in the homogeneity region of $CuInSe_2$ (mainly from $\mu_{Cu}\simeq -0.5$ to 0 eV, from $\mu_{In}\simeq -1.5$ to -0.8 eV),[49] the formation enthalpy of Fe_{In} becomes smaller than $\Delta H(Fe_{Cu})$, whatever the Fe chemical potential. There is only a small part within the $CuInSe_2$ existence region ($\mu_{Cu}-\mu_{In}\leqslant 0.2$ eV) for which Cu substitution has a lower formation enthalpy.

These examples stress the importance of the magnetic interactions in the relative stability of the compounds. Indeed, the nonmagnetic compounds were found in this work to be much less stable than the magnetic ones for a given composition (for instance, nonmagnetic $CuFeSe_2$ is 0.95 eV less stable than FM $CuFeSe_2$).

Regarding the FM-AFM energy difference (Table IV), the method used (DFT and GGA) may overestimate the value obtained, as Ciofini *et al.*[50] have recently shown using a new generation of functionals applied to $KNiF_3$ and K_2NiF_4 insulators. Nevertheless, for almost all the Fe_{Cu} cases studied and some of the Fe_{In} configurations, the energy differences are rather small (smaller than 25 meV), the uncertainty may be important, but the energy differences should remain small.

According to our calculations, the behavior of Fe in $CuInSe_2$ is different from that of Mn in $CuGaSe_2$ as studied by Picozzi *et al.*[33] Mn was found to preferentially substitute to the Ga cation (3+) and the FM ground state was found to be the most stable. The FM ground state for Fe and the AFM one for Mn has also been obtained in the III-V GaAs semiconductor by Sandratskii and Bruno.[35] For our chalcopyrite compound, Fe has the same FM ground state and the magnetic ground state seems to be mainly dependent on the magnetic impurity rather than on the host semiconductor compound.

Our conclusions, based on formation energies, is that Fe_{Cu} substitution is more favorable than Fe_{In}. Nevertheless, in the stability region of $CuInSe_2$, the Fe_{In} formation enthalpy is lower than the Fe_{Cu} one and Fe will preferentially substitutes to In.

The donor or acceptor characteristics of the defects have then been determined from the analysis of the magnetic moment and the charge of the Fe atoms. The electronic defect type is evaluated from the analysis of the total magnetic moments of the supercell and the integral of the DOS and PDOS. They indicate that the ionic charge of the Fe atom in substitution is 3+ for Fe_{In} (magnetic moment of $5\mu_B$) and 1+ for Fe_{Cu} substitution (magnetic moment of $3\mu_B$). For Fe_{In}, the charge is in agreement with what could be expected as the In charge is 3+ in pure $CuInSe_2$. For Fe_{Cu}, the charge is also the same as the charge carried by the Cu atom (1+), and Fe does not have the 2+ or 3+ charge usually carried by Fe atoms. The relative electronegativity can explain this behavior. Fe electronegativity is between the Cu and In electronegativity [χ(Cu)=1.9, χ(Fe)=1.8, χ(In)=1.7, χ(Se)=2.4 (Ref. 51)]; consequently Fe behaves as the substituted cation. Thus, the Fe substitution of In behaves as an acceptor defect (the ionic charge of Fe is 3+ and this cation can accept one electron and give one hole according to $Fe_{In}^{III}\rightarrow Fe_{In}^{II}+h^+$), while the substitution of Cu leads to the formation of a donor defect (the ionic charge of Fe is 1+) and this cation can give one electron according to $Fe_{Cu}^{I}\rightarrow Fe_{Cu}^{II}+e^-$).

In this calculation, two levels due to Fe can be expected to be localized within the $CuInSe_2$ gap, one above the Fermi level when substituting Fe by In and one below for Fe_{Cu}. These levels will form bands at large concentrations (starting below the lowest concentration investigated in this work) as shown in Figs. 6, 7, and 9.

This statement assumes that the gap underestimation of 1 eV for $CuInSe_2$ is almost equivalent to a shift of the conduc-

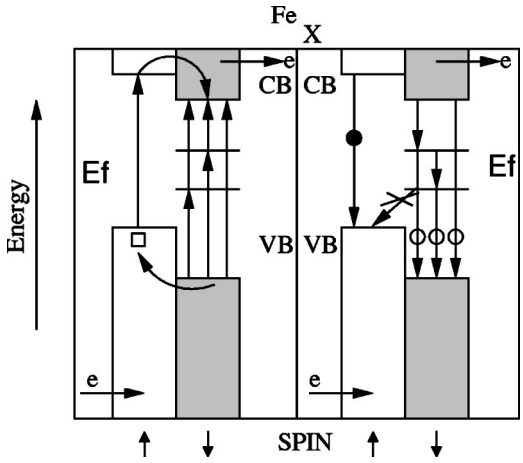

FIG. 10. Schematic electronic transition of Fe-doped $CuInSe_2$ for Fe_X. If X=Cu the Fermi level is above the Fe states, and if X=In E_F is below the Fe states.

tion band by 1 eV.[25] It assumes also that the states associated with Fe are not affected by this well known gap underestimation and may have the same energies compared to the states of the valence band.

The analysis of the electronic structure using the density of states shows that both the charge and the spin are important to account for the semiconductor's properties. Depending on the Fe substitutional site (for concentration smaller than 12.5%), only one spin character (spin down states) is present for a total of two electrons per Fe atoms above (below) the Fermi level for the Fe_{In} (Fe_{Cu}) substitution cases. Therefore a change in the number of electrons (e.g., via doping) will affect the magnetism. The electronic structure of Fe-doped $CuInSe_2$ obtained from the calculated DOS is presented in Fig. 9.

For the previously described low Fe concentration, the density of states is very small at the Fermi level, and becomes large with a significant difference between the up and down density at high Fe concentrations. Thus, these two substitution cases may lead to spintronic effects[13] (requiring a single spin character around the Fermi level) only at concentrations larger than 10%.

In addition, the presence of one Cu vacancy associated with one Fe_{Cu} substitution may move the Fermi level between the two-electron peaks (one electron per peak) which were just below the Fermi level for Fe_{Cu}. This leads to the formation of a semimetallic ground state, which may have also good spintronic properties. The calculation of the DOS with one Fe_{Cu} and one V_{Cu} in a 64-atom supercell confirms that the Fermi level lies in the middle of the two-electron spin-down peak. Because of the antibonding character of the top of the valence band,[29] made from Cu d states, Cu vacancies are in principle easy to form in the chalcopyrite systems, and are usually the easiest defect to form.

The consequences of the Fe-related defect in CIS on the optical transitions are shown in Fig. 10. This is not the situation presented in Fig. 1 because the gap states are both with the same spin state. No transfer between defect semibands able to reduce recombination is therefore expected. Consequently, one is left only with a likely increased recombination rate brought by these defects without any expected benefit. The magnetically doped chalcopyrite system may thus not be the best choice for photovoltaic applications as the band structure is not suitable, but the adjunction of Fe may lead to a spintronic material. A good system to study the potential of magnetically induced inhibition of recombination could be GaN_xO_{1-x},[52] where an intermediate band near optimal optical transition values can be found for some compositions and where ferromagnetic impurities can lead to the desired splitting, provided such compounds can be made with high enough Curie temperatures. Moreover, this compound contains relatively light elements and the spin-orbit interaction is expected to be small, potentially leading to effectively slowed down recombination rates, when they involve spin flipping.

V. CONCLUSIONS

We have performed density functional calculations on the $CuInSe_2$ chalcopyrite and its Fe-doped derivative compounds at different concentrations. The analysis of the defect formation energies indicate that the Fe_{In} substitution is the most favorable in the homogeneity region of CIS, whereas the Fe_{Cu} substitution is slightly more favorable than the Fe_{In} substitution for the cation-rich compound ($\mu_{Cu}=\mu_{In}=0$). The substitution of In by Fe creates structural deformation (a decrease of a and c parameters and a modification of the tetrahedral angles is observed), while Fe_{Cu} substitution does not lead to an important relaxation of the structure.

For Fe_{In}, the ground state is antiferromagnetic for all the concentrations investigated. However for Fe_{Cu} the AFM or FM ground state depends on the concentration and the configuration of the Fe atoms. In all the cases, the energy difference between the FM and AFM states is small and leads to transition temperatures within the 30-400 K range. In addition, it was found that the relative arrangement of magnetic pairs has a strong influence on the coupling constants and the temperatures.

The effect of this substitution on the electronic structure of the compounds is to fill the gap between −3 and −2 eV and to create states above the Fermi level. It is thus an acceptor effect. Our results show that the substitution of In by Fe stabilizes the antiferromagnetic phase when the percentage of substitution is larger than 20%. We believe that this effect can be extended to lower percentages, even though the dimension of the cell size did not permit exploration of these ranges.

We also found that Fe-doped CIS is unlikely to have attractive photovoltaic conversion efficiencies at high Fe concentrations. However, it could have potential applications in spintronic devices, especially if the iron can be substituted for copper, a state presumably easier to achieve in the presence of Cu vacancies, i.e., under growth conditions with low Cu chemical potential. A closer examination of the influence of magnetic elements on the DOS of semiconducting alloys needs to be further investigated in order to see which magnetic-element–semiconductor association could lead to a significant improvement of the conversion efficiency.

ACKNOWLEDGMENTS

This work was carried out with the support of CISEL project funded by ADEME, EDF R&D and CNRS. The authors acknowledge fruitful discussions with V. Cros, H. Jaffres, C. Adamo, and C. Becquart. Part of the calculations have been performed at CEA Grenoble and CCRT Bruyères le Chatel under an EDF-CEA contract.

*Author to whom correspondence should be addressed. Electronic address: jf-quillemoles@enscp.jussieu.fr

[1] M. A. Contreras, B. Egaas, K. Ramanathan, J. Hiltner, A. Swartzlander, F. Hasoon, and R. Noufi, Prog. Photovoltaics **7**, 311 (1999).
[2] J. Hedstrom, H. Ohlsen, M. Bodegard, A. Kylner, L. Stolt, D. Hariskos, M. Ruckh, and H.-W. Schock, presented at the *23rd IEEE Photovoltaic Specialists Conference, 1993*, Louisville, KY (IEEE Press, Piscataway, 1993).
[3] T. Negami, M. Nishitani, N. Kohara, Y. Hashimoto, and T. Wada, Mater. Res. Soc. Symp. Proc. **426**, 278 (1996).
[4] K. Zweibel, Prog. Photovoltaics **3**, 279 (1995).
[5] F. Karg, H. Aulich, and W. Riedl, in *Proceedings of the 14th European Photovoltaic Solar Energy Conference, 1997*, Barcelona, edited by H. A. Ossenbrink, P. Helm, and H. Ehmann (H.S. Stephens and Associates, Bedford, UK, 1997).
[6] B. Dimmler and H. W. Schock, Prog. Photovoltaics **4**, 425 (1996).
[7] J. F. Guillemoles, P. Cowache, A. Lusson, K. Fezzaa, F. Bonvoisin, J. Vedel, and D. Lincot, J. Appl. Phys. **79**, 7293 (1996).
[8] D. Guimard, N. Bodereau, J. Kurdi, J. F. Guillemoles, D. Lincot, P. P. Grand, M. BenFarrah, S. Taunier, O. Kerrec, and P. Mogensen, in *Proceeding of the 3rd conference on photovoltaic energy conversion, 2003*, Osaka, Japan, edited by Kurohawa (IEEE Press, Pistacaway, 2003), 2P-P3-58.
[9] B. A. Anderson, Prog. Photovoltaics **8**, 61 (2000).
[10] J. F. Guillemoles, L. Kronik, D. Cahen, U. Rau, A. Jasenek, and H. W. Schock, J. Phys. Chem. B **104**, 4849 (2000).
[11] V. Aubin, L. Binet, P. Stallworth, and J. F. Guillemoles, J. Phys. Chem. Solids **64**, 1633 (2003).
[12] T. Dietl, H. Ohno, F. Matsukura, J. Cibert, and D. Ferrand, Science **287**, 1019 (2000).
[13] G. Schmidt, D. Ferrand, L. W. Molenkamp, A. T. Filip, and B. J. van Wees, Phys. Rev. B **62**, R4790 (2000).
[14] I. Zutić, J. Fabian, and S. Das Sarma, Rev. Mod. Phys. **76**, 323 (2004).
[15] W. Shockley and H. J. Queisser, J. Appl. Phys. **32**, 510 (1961).
[16] G. L. Araujo and A. Marti, Sol. Energy Mater. Sol. Cells **33**, 213 (1994).
[17] G. L. Araujo and A. Marti, Sol. Energy Mater. Sol. Cells **43**, 2013 (1996).
[18] A. S. Brown and M. A. Green, J. Appl. Phys. **92**, 1329 (2002).
[19] G. Yu, J. Gao, J. Hummelen, F. Wudl, and A. J. Heeger, Science **270**, 1789 (1995).
[20] M. Granstrom, K. Petrisch, A. C. Arias, A. Lux, M. Anderson, and R. H. Friend, Nature (London) **295**, 257 (1998).
[21] W. C. Chou, A. Petrou, J. Warnock, and B. T. Jonker, Phys. Rev. B **46**, 4316 (1992).
[22] R. Fiederling, M. Keim, G. Reuscher, W. Ossau, G. Schmidt, A. Waag, and L. M. Molenkamp, Nature (London) **402**, 787 (1999).
[23] A. Luque and A. Marti, Phys. Rev. Lett. **78**, 5014 (1997).
[24] S. Kettemann and J. F. Guillemoles, in *Proceedings of the 13th European PV Solar Energy Conference, Nice, 1995*, edited by W. Freienlebens, W. Palz, H. A. Ossenbrink, and P. Helm (H.S. Stephens and Associates, Bedford, UK, 1995), p. 119.
[25] S. B. Zhang, S. H. Wei, A. Zunger, and H. Katayama-Yoshida, Phys. Rev. B **57**, 9642 (1998).
[26] S. H. Wei, S. B. Zhang, A. Zunger, and H. Katayama-Yoshida, J. Appl. Phys. **85**, 7214 (1999).
[27] J. E. Jaffe and A. Zunger, Phys. Rev. B **28**, 5822 (1983).
[28] C. Domain, S. Laribi, S. Taunier, and J. F. Guillemoles, J. Phys. Chem. Solids **64**, 1657 (2003).
[29] C. Domain, J. M. Raulot, S. Laribi, S. Taunier, and J. F. Guillemoles, MRS Proc. **763**, B8.10.1 (2003).
[30] J. A. Rodríguez, L. Quiroga, A. Camacho, and R. Baquero, Phys. Rev. B **59**, 1555 (1999).
[31] J. E. Jaffe and A. Zunger, J. Phys. Chem. Solids **64**, 1547 (2003).
[32] Y. J. Zhao and A. Zunger, Phys. Rev. B **69**, 075208 (2004).
[33] S. Picozzi, Y. J. Zhao, A. J. Freeman, and B. Delley, Phys. Rev. B **66**, 205206 (2002).
[34] L. M. Sandratskii and P. Bruno, Phys. Rev. B **67**, 214402 (2003).
[35] L. M. Sandratskii and P. Bruno, Phys. Rev. B **66**, 134435 (2002).
[36] C. Parlak and R. Eryigit, Phys. Rev. B **66**, 165201 (2002).
[37] P. Hohenberg and W. Kohn, Phys. Rev. **136**, B864 (1964); W. Kohn and L. Sham, Phys. Rev. **140**, 1133 (1965).
[38] J. Hafner, Acta Mater. **48**, 71 (2000).
[39] G. Kresse and J. Hafner, Phys. Rev. B **47**, 558 (1993); **49**, 14251 (1994).
[40] G. Kresse and J. Furthmüller, Phys. Rev. B **54**, 11169 (1996).
[41] G. Kresse and J. Furthmüller, Comput. Mater. Sci. **6**, 15 (1996).
[42] D. Vanderbilt, Phys. Rev. B **41**, 7892 (1990); G. Kresse and J. Hafner, J. Phys.: Condens. Matter **6**, 8245 (1996).
[43] J. P. Perdew and Y. Wang, Phys. Rev. B **45**, 13244 (1991).
[44] H. J. Monkhorst and J. D. Pack, Phys. Rev. B **13**, 5188 (1976). In the original Monkhorst-Pack scheme, the k point mesh is always symmetric around the Γ point, whereas very often in our calculations we adopted grids centered at the Γ point.
[45] K. S. Knight, Mater. Res. Bull. **27**, 161 (1992).
[46] J. Parkes, R. D. Tomlinson, and M. J. Hampshire, J. Appl. Crystallogr. **6**, 414 (1973).
[47] G. Sanchez Porras and S. M. Wasim, Phys. Status Solidi A **133**, 509 (1992).
[48] C. Kittel, *Introduction to Solid State Physics*, 6th ed. (Wiley, New York, 1987).
[49] J. F. Guillemoles, Thin Solid Films **361-362**, 338 (2000).
[50] I. Ciofini, F. Illas, and C. Adamo, J. Chem. Phys. **120**, 3811 (2004).
[51] L. Pauling, *The Nature Chemical Bonds* (Cornell University Press, Publisher, 1967), p. 267.
[52] K. M. Yu, W. Walukiewicz, J. Wu, W. Shan, J. W. Beeman, M. A. Scarpulla, O. D. Dubon, and P. Becla, Phys. Rev. Lett. **91**, 246403 (2003).